INTERNATIONAL SCIENTIFIC AND VOCATIONAL JOURNAL (ISVOS JOURNAL)

Vol.: 3 Issue: 2 Date: December 2019 Received:23.08.2019 Accepted:21.11.2019 Final Version: 31.12.2019

ISVOS Journal, 2019, 3(2): 92-104

Automated Diagnosis of Meniscus Tears from MRI of The Knee

Ahmet Saygılı[a, 1], Songül Varlı[b]

[a] Tekirdağ Namık Kemal University, Çorlu Engineering Faculty, Department of Computer Engineering, Silahtarağa Mh., 59860 Çorlu, Tekirdağ

[b]Yıldız Technical University, Computer Engineering Department, Yıldız Mh., 34349, Davutpaşa, İstanbul

Abstract

Meniscus tears are serious knee abnormalities that can cause knee osteoarthritis disorder. Therefore, early detection and treatment of meniscus tears that may occur in the knee with computer-aided systems will prevent the progression of these disorders. In this study, an approach which can detect the meniscus tears automatically by using and comparing two different feature extraction methods have been presented. With these methods, features of the knee MR images were obtained and such features performed automatic meniscus tear classification. Four different classifiers have been used to model the features in the classification phase. The most successful classification results were obtained from the support vector machines (SVM) with a success rate of 90.13% and the extreme learning machines (ELM) with a success rate of 87.85% via the LBP feature extraction method. It is observed that better results are obtained than the ones in similar studies in the literature. It is aimed to improve the existing success with the use of deep feature extraction methods in the future.

Keywords: "Diagnosis; Knee Joint; HOG, LBP; Meniscus Tear; Medical Image Processing"

1. Introduction

Computer-aided diagnostic (CAD), design and engineering studies have increased considerably in recent years [1, 2]. Because such studies support people from medical science in their decisions. In particular, studies in the field of medical imaging contribute to radiology and orthopedic specialists. In this study, MRI images of the knee were analyzed and the CAD system was created to provide support to radiology and orthopedic specialists. The knee joint is responsible for providing mobility in the human body. Any discomfort that may occur in the knee joint may restrict its ability to move. Especially osteoarthritis (OA) is a severe discomfort affecting the knee joint as it affects many joints in the body. Early diagnosis and treatment of this condition play a major role in preventing the disease. This is one of the most important reasons for utilizing computer-assisted automatic detection systems. In addition, the experience of radiology specialists in assessing the output of imaging devices also plays a role in determining these conditions. Other significant purposes of the work in this field are reducing the faulty evaluations that radiologists will make and producing the systems that can support them in their decisions. Because of these reasons, computer-aided diagnosis and detection systems are developed. Image processing techniques are generally used in these systems. In particular, feature extraction methods play an important role in the success of the work carried out in this area.

Different feature extraction methods are used according to the problem type of image processing. HOG [3] and LBP [4, 5] are two methods that provide successful results in solving different problems in feature extraction. In the literature, there are studies in which these two methods are successfully applied to various fields such as medical image processing, object and pattern recognition. Especially, HOG and LBP are frequently used in both face recognition and face expression [6-8]. In addition to these methods, Gabor filters [9], Scale Invariant Feature Transform (SIFT) [10] and Speeded-up Robust Features (SURF) [11] are the other methods that are often preferred for feature extraction. On the other hand, when the feature extraction methods are used together, it is observed that successful results are obtained [12], [13]. HOG and LBP are prominent feature extraction methods due to their low memory and computational cost. These methods are tolerant of image transformations such as illumination changes. In this study, we compared the strengths and weaknesses of these feature extraction methods and their comparative results on a knee MR image data set.

[1] Sorumlu Yazar. Tel.: +90-282-250-2300; fax: +90-282-250-9924 .
E-posta adresi: asaygili@nku.edu.tr

Section 2 introduces the knee joint and anomalies. Section 3 introduces the materials and methods. Experimental results are in Section 4, while discussions are in Section 5. Finally, the contributions of the study and suggestions for future work present in Section 6.

2. Knee Joint

The knee joint consists of bones, articular cartilage, and meniscus. Each of these components directly affects the ability to move. The meniscus tissues are half-moon-shaped structures between the tibia and femur bones. [14]. The most important task of them is to reduce the load on the knee [15]. There are two types of meniscus in the human body, namely medial and lateral, in each knee joint. Meniscus tears often cause cartilage and bone deterioration in the knee joint. Another task of the meniscus is to protect the joint cartilage. Its main function is to maximize the contact area within the tibia-femoral joint and minimize contact stress. The contact mechanism of this joint can easily change due to meniscus tears. Furthermore, the structure of articular cartilage metabolism may be disrupted and this puts the array at risk for early osteoarthritis [16]. Meniscus tears are a discomfort, especially in younger athletes and older people. Meniscus tears can occur as a result of the movement, commonly known as sudden rotation. The diagnosis of meniscal tears is made by radiologists.

Studies conducted on meniscus have been classified under two topics that are based on meniscus segmentation and automatic determination of meniscus tears. In some studies, both operations are performed. In studies that do not detect meniscal tears but only focused on segmentation studies, the main purpose is to segment the meniscus tissues that were manually segmented by radiologists [17-22]. In meniscal tear involved studies, the aim is primarily to segment the meniscus, determine its location and then to detect tears.

Computer-aided detection of meniscal tears has been increasing in recent years. The study by Hata et al. was the first study on meniscus tears [23]. In this study, a system, for the diagnosis of meniscus tears on the knee MR images in the sagittal plane, was presented. This study was lacking manual determination of meniscus tears by an expert. Another study was performed on fifty-five MR images [24]. A region growing approach was adopted to determine the location of menisci. At the end of the study, the menisci were classified as either normal or damaged by using the Bayes classifier with an accuracy of 89%. The missing aspects of this study were those (i) it did not detect a torn meniscus (level 3), and (ii) it only detected the posterior horns of the medial meniscus. Sagittal knee MR images were used in another study, in which, meniscus tissues were segmented by a histogram-based approach and tears were tried to be detected by the template matching method [25]. Using this region-specific assumption in determining the meniscus' location can be considered as a shortcoming. A computer-assisted automated process to detect meniscal tears and leveling tears was also performed on MR images by Ramakrishna et al. [26]. Additionally, Fu et al. conducted another computer-assisted study to detect meniscus tears [27]. In the study, the Active-Contour with Level Sets method was used to determine meniscus's location. Then, they have extracted features for suspicious meniscus from both the spatial and spectral planes. The as-obtained features were classified by SVM classifier and meniscus tears were detected [27]. Zarandi et al. performed a study to diagnose meniscal tears in 2016 [28]. In Zarandi's study, MR images were firstly segmented by both Fuzzy C-Means (FCM) and Probabilistic Fuzzy C-Means (PFCM) clustering methods and then they were classified by perceptron neural network to determine whether MR images were torn. As a result of this study, the medial meniscus anterior horn tears were classified with a success rate of 84.24%. Saygılı et al. segmented the menisci by the FCM method and visualized the meniscus tears in 2017 [29]. Although it was a beginner level study, it will shed light on future studies. We can say that it was conducted on a small dataset and that the validation process was not included.

2.1. Osteoarthritis and meniscal tears

Osteoarthritis (OA) is a common disease worldwide. Technological advances have led OA to play an increasingly important role in the disease process. Radiography is currently the most commonly used imaging modality for imaging-based diagnosis of OA. There is a need for effective non-surgical treatment of OA. However, despite the ongoing research, no drug has been discovered or approved until now to provide a definitive solution to OA. [30]. OA disease is seen in the middle age group and usually people over 65 years old. Osteoarthritis is most commonly seen in the knee joints. The severity of knee osteoarthritis appears to be increased as a result of a 1-year follow-up [31]. If not diagnosed early, it gets worse over time and causes bone structures to wear out [32]. One of the causes of knee osteoarthritis is tears in meniscus structures. Despite extensive clinical trials, there is no common consensus on the classification criteria of knee osteoarthritis [33]. For this reason, automatic detection systems are expected to provide information that can help in this regard. A study has shown that knee OA is associated with pain when standing up or down the stairs [34]. In some studies, analyses such as gait analysis were performed in detecting OA discomfort [35]. Moreover, there are studies that show that osteoarthritis is associated with bone tissue and bone mineral density in the knee [36, 37]. Every year, studies are carried out regularly to evaluate OA discomfort with imaging techniques [38, 39].

Osteoarthritis (OA) is a chronic and painful disease of the knee joint. The most commonly used method for assessing osteoarthritis is MRI. Another common complication in the knee joint is meniscal tears. The meniscal tears usually occur when the knee is bent or when the movement called 'sudden rotation' takes place. These tears can occur when they are lifted heavily or

when doing sports. In older ages, the meniscus wears off. This leads to easier meniscus tears [40, 41]. The diagnosis of meniscal tears is made by radiologists. Manual segmentation of menisci in MR images by radiologists takes about 30-35 minutes [42]. The knee joint needs to be visualized with imaging techniques such as computed tomography and magnetic resonance imaging to allow diagnosis. Early diagnosis of meniscus tears enables physicians to prevent the occurrence of disorders such as osteoarthritis and allow treatment to be delayed [43]. In this study, magnetic resonance images obtained in the sagittal plane in the weDESS standard were used to evaluate the performance of a computer-aided diagnosis system (CAD) that automatically classifies meniscal tears to support radiology specialists.

3. Materials and Methods

The meniscus is crescent-shaped cartilaginous structures. Their major task is to move the load on the knee and reduce the friction. The anomalies that occur in the meniscus directly affect mobility in a negative manner. Therefore, early diagnosis and treatment of such anomalies in the meniscus structure are crucial. For this purpose, computer-aided automatic detection systems have been developed. In the present study, a system that automatically detects meniscus tears was established.

Knee MR images were used to assess meniscal structures in this study. The dataset provided by OAI is open to public access. The dataset contains both healthy and damaged MR images with different degrees of discomfort. In addition, 88 MR images were manually marked to be used for evaluation by the radiologists. Each MR image in the dataset was obtained by high field scanners (3 Tesla) and has 160 slices. The size of each slice image is 384 × 384 pixels. In this study manually marked MR images were used.

This study also focused on the investigation of the effect of HOG and LBP feature extraction methods. For this purpose, it is important to explain the details of feature extraction methods and to discuss the as-obtained results on knee MR images. Thus, HOG and LBP methods will be explained in the following section.

3.1. Obtaining Rectangular Windows

For the classification of the meniscus, firstly the most optimal rectangular windows were obtained. The process is shown in Figure 1.

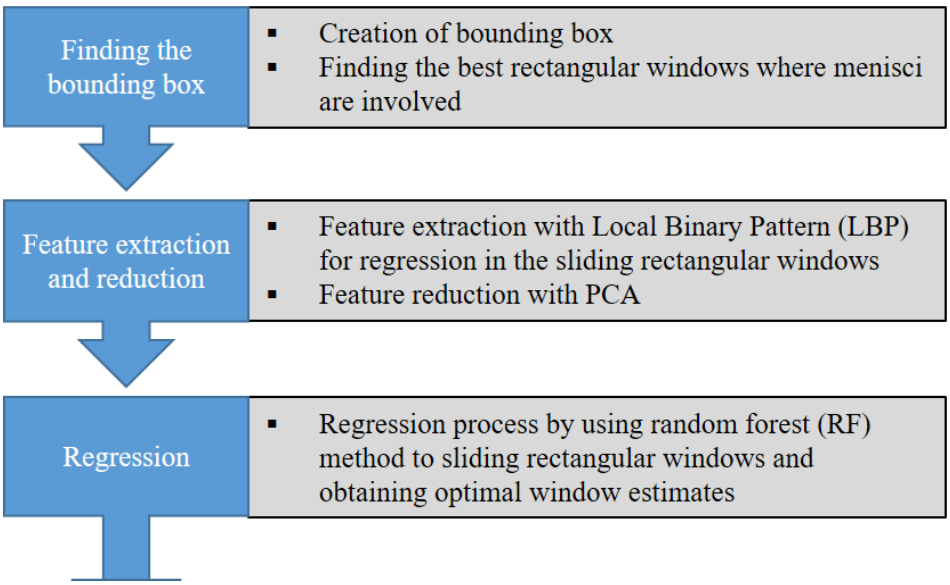

Figure 1. Flowchart for obtaining optimal rectangular windows

Each slice of the MR images in the data set is 384×384 pixels. In Figure 2, the meniscus structures are marked in a rectangular box. The bounding box is shown in white and the optimal rectangles surrounding the menisci are in the bounding box. As you can see, the meniscus is located in a certain and small area.

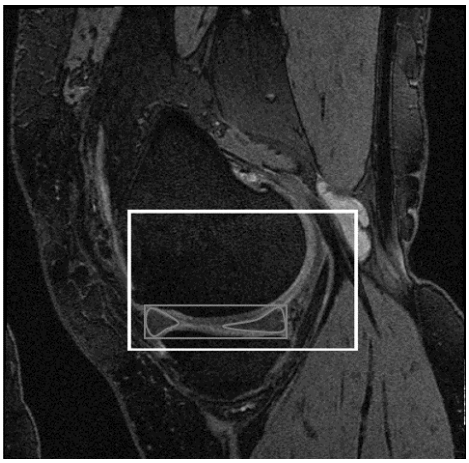

Figure 2. The bounding box (white rectangle), optimal rectangular window and menisci

To reduce the time and cost of operation, it is thought that it would be right to look for a narrowed area instead of searching the meniscus structures completely in the slices. The bounding box was implemented on manually marked MR images in the dataset. The minimum and maximum x-y coordinates of the meniscus are determined by the ground truth data of each MR image. This process was applied to all MR images in the dataset and additionally, +5 pixel padding in row and column was added to obtain the global minimum and global maximum points. At this point, a global bounding box is obtained as in Fig. 2. The resulting bounding box is 188 × 115 pixels in size. This reduces the current search rate by 80%. After this process, the process of finding the windows in which the meniscus is located in the bounding box has been started. In the feature extraction process, the window is shifted by 2 pixels in the bounding box with 50×160 size and the features of the window are extracted by the Local Binary Pattern (LBP) method. In order to be used as a target variable in the regression process, the spatial overlaps of the shifting windows and the actual windows are used as shown in Figure 3.

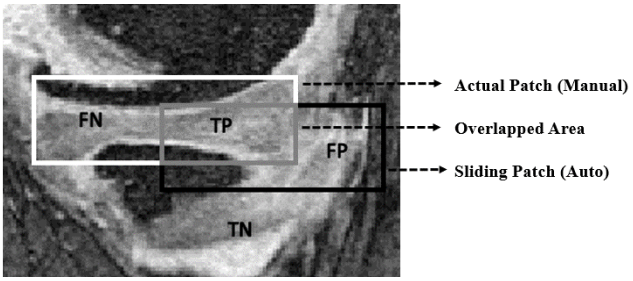

Figure 3. Spatial overlap calculation

Spatial overlap (gray area in Figure 3) has been calculated using the Dice similarity metric shown in Equation 1.

$$\text{Dice} = \frac{2 * \text{TP}}{(2 * \text{TP} + \text{FP} + \text{FN})} * 100 \quad (1)$$

TP, FP, and FN mean the true positive, false positive and false negative, respectively. Figure 4 shows the distributions of the spatial overlap ratios from the bounding boxes. When we look at the figure, it is seen that the overlap ratio of an excess of about 150,000 samples obtained for an image is within the range of [0, 0.1]. However, there are quite a few examples where the overlap area ratio is [0.8, 0.9]. Looking back at Figure 2, it appears that the area outside the actual meniscus window is quite large.

In order to reduce the computation time, a reduction was made in these samples. The samples were selected which were below the cut line determined according to the specific threshold value shown in Figure 4. The number of samples remaining under this line is randomly selected for each interval. That is, it is seen that there are about 80,000 samples in [0, 0.1] range. 1000 specimens were randomly selected from these 80,000 samples for the identification of 1000 samples remaining under the line.

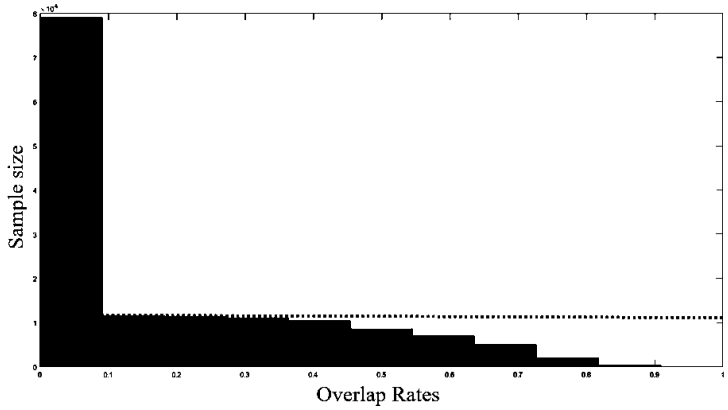

Figure 4. An example of the histogram of overlap ratios for an MR image

After random sub-sampling, approximately 150,000 sample sizes obtained for each MR image were reduced to 7000. Then, in order to obtain the most discriminating feature vector, feature selection was made by the PCA method and 200 features with the highest eigenvalue were selected. After determining the features to be used, the regression method was applied to a random forest (RF) method.

In the study, as the target variable, the actual meniscus windows obtained with the ground truth data, as shown in Figure 3, and the overlap area of prediction windows in the bounding box are used. After this process, features were extracted by the LBP method and implemented to the regression process by the RF method. Thus, windows with meniscus are specified which provide the best overlap for each slice. After obtaining the most optimal rectangular windows for each slice as shown in Figure 5, feature extraction with HOG and LBP was performed from these windows, followed by tear classification with different classifiers.

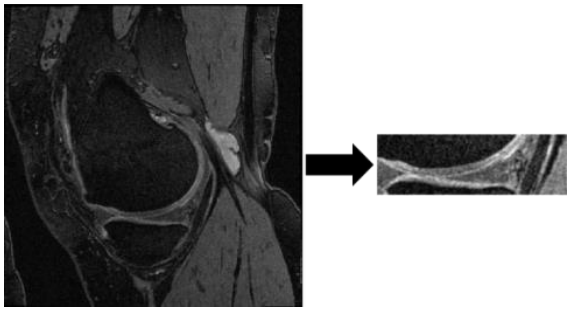

Figure 5. Obtaining rectangular windows

In the following section, we will first explain how feature extraction methods are applied and then the classification process.

3.2. Histogram of Oriented Gradients (HOG)

HOG is a feature extraction method that provides successful results in pattern recognition. In this method, the feature extraction is performed by the gradients and orientations of the pixels on the image. HOG method was actively used in the studies that allow the determination of OA disorders on the knee [29, 44-47].

The steps of the algorithm applied in HOG method are as follows;

1. The calculation of gradient sizes (G) and gradient orientation angles (θ) of the cells in the image, and the extraction of the image edges (G_x and G_y),
2. The use of gradient magnitudes for each pixel to calculate the gradient histograms,
3. Perform block normalization.
4. Obtaining HOG feature vectors.

In order to obtain HOG features, first of all, the gradient (direction vector) magnitude and its orientation angle must be calculated. To do this, the edges of G_x and G_y are determined by applying horizontal and vertical Sobel filters to the image (Equation 2) and then, the G and θ values are calculated as shown in Equation 3.

$$G_x = I * [-1\ 0\ 1], \quad G_y = I * [-1\ 0\ 1]^T \tag{2}$$

$$G = \sqrt{G_x^2 + G_y^2}, \quad \theta = \arctan\frac{G_x}{G_y} \tag{3}$$

The calculated angle (θ) is used as the input value in gradient histograms. For the pixels in each cell, a gradient histogram consisting of 0°-180° or 0°-360° with 20° intervals is generated. Dalal and Triggs have reported that creating an unsigned 9-channel histogram produces better results in their study [3]. Therefore, a 9-channel histogram is also used in this study. The gradient magnitudes calculated for each pixel are used for the calculation of gradient histograms in cells. Here, each pixel is voted on the channel according to the gradient orientation corresponding to the gradient size.

HOG is a robust method against light illumination and variations from shadows. This is achieved by block normalization. In this process, the average pixel values in each cell are taken and applied to the blocks consisting of cells. When HOG features are extracted, 2 × 2 block size is used. Also, the size of each cell in the block is set to 10 units. This means that in both x and y directions, the window is divided by 10 × 10 cells and the descriptors for each cell are calculated. An example HOG obtained from the selection of cell size 10 is shown in Figure 6.

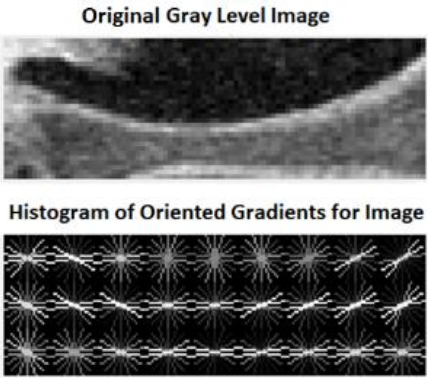

Figure 6. Visualization of HOG for a meniscus tissue

3.3. Local binary patterns (LBP)

LBP is a non-parametric feature extraction method [4, 5]. The LBP can be described as the orthogonal measure of local contrast. Initially, it was introduced as a tissue pattern analysis technique. The fact that LBP has significant advantages, such as high tolerance to images with different lighting conditions, sensitivity to small changes in gray-level images and low computational costs that make it a frequent choice in image processing studies [48]. It is also used actively in the studies that allow the detection of OA discomfort on the knee [49, 50].

The basic steps of the algorithm applied in the LBP method are as follows;

1. Split sub-images of the original image into smaller sizes: "cells". (E.g. 16 × 16 pixels for each cell)
2. Compare each pixel in a cell to its neighbors (left top, left middle, bottom left, top right, etc.).
    a. Neighborhoods are generally (8, R) and (16, R). Here R is the distance to the neighbors. 8 and 16 indicate the number of neighbors.
3. Track the pixel along a clockwise or counterclockwise circle,
    a. Write "0" if the value of the middle pixel is greater than or equal (≥) to the value of the neighbor, otherwise write "1".
        i. If the result of this operation looks at 8 adjacencies, generate an 8-digit binary number.
        ii. Generally, for convenience, the resulting binary number is converted to a decimal number.

4. Calculate the histogram of each number frequency in the cell (this histogram is a feature vector of 256 dimensions)

    a. Obtain 59-dimensional uniform patterns from the feature vector of 256 dimensions based on bitwise.

    b. Obtain the merged (normalized) histograms of all cells (this gives a feature vector for the whole view).

The LBP identifier is calculated by using Equation 4;

$$LBP_{P,R}(x_c) = \sum_{p=0}^{P-1} u(x_p - x_c)2^p, u(y) = \begin{cases} 0, & \text{if } y < 0 \\ 1, & \text{if } y \geq 0 \end{cases} \quad (4)$$

x_c = central pixel, x_p = neighbors of the central pixel, R = distance of the central pixel to the neighbor pixels, P = neighboring number.

According to Equation 4, 2P different LBP codes are generated for P-bit binary numbers. For example like the 8-bit, there are 28 = 256 different patterns. Some of these patterns obtained in LBP are divided into two groups as uniform and non-uniform. In many tissue analysis applications, it is desirable to obtain invariant properties against the rotation of the input image [51]. Since the LBPP, R patterns are obtained by a circular sampling around the center pixel, the rotation of input image has two effects; (i) each local neighborhood is rotated to other pixel locations, and (ii) the sampling points surrounding the center pixel in each neighborhood are rotated in a different direction. In many applications, uniform patterns, which are the different extensions of LBP, are used [52]. For this, a uniformity criterion that indicates the number of bitwise passes from 0 to 1, is defined. A local binary pattern is defined as uniform if the uniformity criterion is maximum 2. For example, 00000000 (0 transition), 00011100 (2 transition) and 11101111 (2 transition) are uniform. However, 00110100 (4 passes) and 01010100 (6 passes) are non-uniform patterns. In uniform LBP mappings, there is a distinct output label for each uniform pattern, and all non-uniform patterns are appointed as a single label. Thus, the number of different output labels will be P(P-1)+3 for mapping the patterns with P bites. For example, for the neighbors of 8 sampling points, the number of output labels would be 59, and for 16 sampling points, it will be 243.

There are two different reasons for removing non-uniform patterns. First of all, in natural images, most of the local binary patterns are uniform. Another reason for creating uniform patterns is statistical robustness. The use of uniform patterns instead of all possible patterns produces better recognition results in many applications [53].

LBP method is often preferred because of its; conformity to the anatomical structure of medical images, contrast-based feature extraction, high tolerance for images with different lighting conditions, sensitivity to small changes in gray-level images, and its low memory cost compared to the other methods. An example of the LBP features obtained from the knee MR images in this study is shown in Figure 7. When the LBP feature vectors are viewed in this figure, it can be seen that the textural features of the meniscus structures and the background are successfully demonstrated.

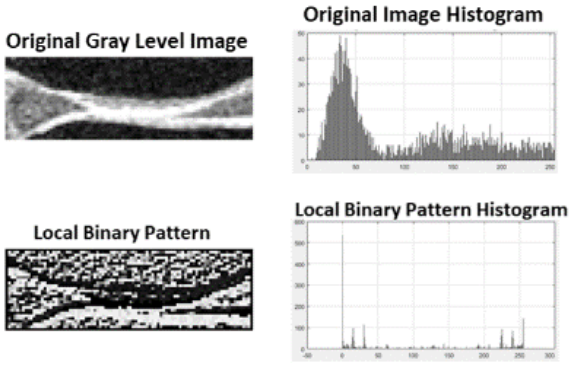

Figure 7. Visualization of LBP features in a sample meniscus window

As a result of previous experimental studies that worked on different window sizes and memory dimensions, in this study, the LBP cell size was determined to be 10.

4. Experimental Results

In this study, knee MR images with open access by the OAI were used as input to compare the classification success achieved with the HOG and LBP methods according to different classifiers [54]. Here, the most compact meniscus windows obtained from the knee MR slices were used.

In the study performed, descriptors obtained by HOG and LBP methods were modeled with k-nearest neighbors (k-NN), support vector machines (SVM), extreme learning machines (ELM) and random forest (RF) classifiers to determine whether the meniscus in the knee MR images was torn. The distance metric for k-NN is Euclidean and the k is 5. 4096 hidden layers and the sigmoid activation function are defined for the ELM. A radial basis function was used for SVM. The tree size is determined as 20 and the number of features to sample is set to one-third of dimensionality for random forest method. The leave-one-out cross-validation technic was used for the classification phase.

The classification results are shown in Table 1. When the table is examined, the most successful classifier is seen as SVM and that it is followed by ELM. When the feature extraction methods are compared with the results on the table it can be seen that the LBP method is better suited for the as-used dataset. Especially when the results obtained by the SVM are taken into consideration, it can be observed that the performance value is 90.13% when the features are obtained by the LBP method, while 86.48% performance is achieved in the HOG case.

Table 1. Classification results obtained by different classifiers and feature extraction methods

		k-NN	SVM	ELM	RF
HOG	Accuracy (%)	82.91	86.48	86.22	77.55
	Sensitivity (%)	91.26	88.83	91.02	72.82
	Specificity (%)	73.66	83.87	80.91	82.80
LBP	Accuracy (%)	86.58	90.13	87.85	76.45
	Sensitivity (%)	87.68	90.64	89.41	75.86
	Specificity (%)	85.42	89.58	86.20	77.08

In order to increase the comparability and understanding of feature extraction methods, Table 1 is transformed into a column graph as shown in Figure 8.

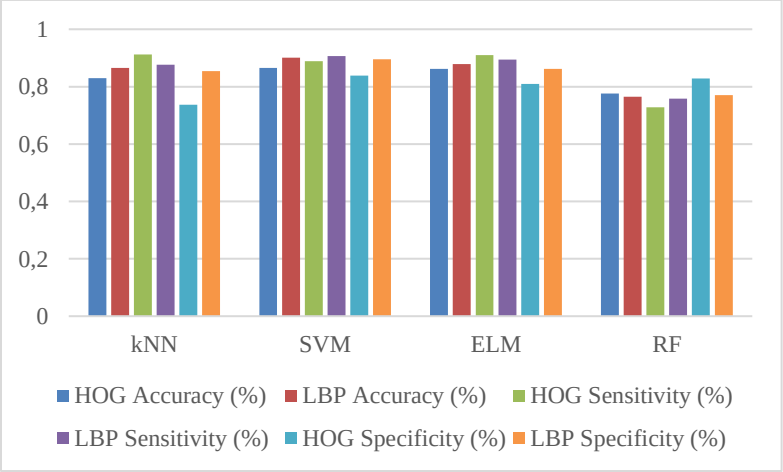

Figure 8. Comparison of feature extraction methods

In Table 2, it is possible to see the implementation times for two different classifiers of the HOG and LBP methods. As shown in the table, the LBP method is about two times faster than the HOG method. On the other hand, given the fact that radiologists spend 35 minutes evaluating a single MR image [55], it appears that the realization times achieved here are rather low.

Table 2. The implementation times for two different classifiers of the HOG and LBP methods

	HOG + SVM	HOG + RF	LBP + SVM	LBP + RF
Training Time (Seconds)	2868 s	2955 s	2993 s	1110 s
Testing Time (Seconds)	4.09 s	3.19 s	3.79 s	3.03 s

5. Discussions

In this study, HOG and LBP feature extraction methods were used to process the knee MR images. When the results were examined, it was seen that both LBP and HOG method obtained very successful results in the classification of MR images. It has been found that the classification performance obtained by the LBP method is better than the HOG method.

Table 3. Comparison summary of the relevant previous studies in the literature

Author(s)	Year	Method	Success Rate (%)
Boniatis et al.	2008	Region Growing and Bayes Classification	Accuracy: 89.1 Sensitivity: 92.5 Specificity: 80.0
Köse et al.	2009	Histogram-based approach Statistical segmentation approach	Accuracy for diseased participants: 88.3 Accuracy for healthy participants: 95.7
Ramakrishna et al.	2009	Thresholding, area and surface constraints	Sensitivity: 83.87 Specificity: 75.19
Fu et al.	2013	Active contour model, SVM	Sensitivity: 72.7
Zarandi et al.	2016	Fuzzy c-means, Neural network	Specificity: 88.82-92.13
This Study	2019	HOG and LBP k-NN, ELM, RF, and SVM	Accuracy: 90.13 Specificity:90.64 Sensitivity:89.58

A comparison of studies performed on the detection of menisci is shown in Table 3. It is possible to see the methods and the success rates of the works in this table. It would not be wrong to say that the results of the present work are comparatively better than the other ones.

Ramakrishna presented an automated computer-aided diagnosis system for MR images with low field scanners in their work. When we compared this study with our work, too much preliminary information was used. For example, the choice of slices is manually determined by radiologists. The system they are applying is overly dependent on the data set they use. This system is very unlikely to be applied to a different set of data. Fu et al. are used active contour with level set modeling approach, followed by a system that identifies meniscus tears by extracting features with co-occurrence matrices and classifying them with support vector machines. The sensitivity value of 72.7% is far from our work. Zarandi et.al.'s work in 2016 performed segmentation

using fuzzy clustering approaches and performed classification with perceptron neural networks. The use of proton weighted excitation sequences showed better results in the detection of meniscal tears than the weDESS. At the same time, it is thought that evaluations in the coronary and axial plane may present different perspectives in studies related to meniscus tears.

Here, the achieved success is higher since the completion time of a process, which has taken 35 minutes by radiologists, seems to take quite shorter in the automatic system used in this study as shown in Table 2. Thanks to this system, an approach has been created to support radiology specialists in their decisions. Compared with the studies carried out in the literature, it is seen that the execution time of this study is quite good. Early diagnosis and treatment of structures in the knee joint significantly affect the detection of the disease. For this reason, we have been able to make the decisions that radiologists will make in a shorter time. On the other hand, MR reader variability faults will be reduced by this study. Another factor contributing to the study is the success rate achieved. It has to be said that the realization of different feature extraction methods and classifiers contributes to this situation. A detailed analysis of the feature extraction methods used in the study will also contribute to the researchers working in this area.

6. Conclusions

Detection of anomalies in deformable structures such as meniscus is difficult. There is no standard shape for the meniscus on the slices, so this situation also makes the detection difficult. On the other hand, the contrast of neighboring structures such as meniscus and cartilage is close to each other, so that it is possible to make mistakes in distinguishing these structures from each other. A new system has been proposed to detect the tears of the meniscus structures in the knee joint. A comprehensive analysis of the HOG and LBP feature extraction method in the proposed system should be emphasized. Early diagnosis and treatment of the knee joint are very important in determining the meniscus tears in a very short time is one of the most effective parts of the study. It is also worth mentioning that it is a work that can be used as a decision support system for radiology specialists. Computer-aided automatic modules are expected to be available in imaging devices in the near future. In this way, we can say that the positive contributions of working. In the next step, it is aimed to create a system in which hybrid feature extraction methods are used to determine the types of meniscal tears.

7. References

[1] B. Öztürk, L. Uğur, F. Erzincanlı, and Ö. Küçük, "Optimization of Polyethylene Inserts Design Geometry of Total Knee Prosthesis," *International Scientific and Vocational Studies Journal,* vol. 2, pp. 31-39.

[2] A. Saygılı, "Classification and Diagnostic Prediction of Breast Cancers via Different Classifiers," *International Scientific and Vocational Studies Journal,* vol. 2, pp. 48-56.

[3] N. Dalal and B. Triggs, "Histograms of oriented gradients for human detection," in *2005 IEEE Computer Society Conference on Computer Vision and Pattern Recognition (CVPR'05)*, 2005, pp. 886-893 vol. 1.

[4] T. Ojala, M. Pietikäinen, and D. Harwood, "A comparative study of texture measures with classification based on featured distributions," *Pattern recognition,* vol. 29, pp. 51-59, 1996.

[5] T. Ojala, M. Pietikainen, and D. Harwood, "Performance evaluation of texture measures with classification based on Kullback discrimination of distributions," in *Pattern Recognition, 1994. Vol. 1-Conference A: Computer Vision & Image Processing., Proceedings of the 12th IAPR International Conference on*, 1994, pp. 582-585.

[6] P. Carcagnì, M. Coco, M. Leo, and C. Distante, "Facial expression recognition and histograms of oriented gradients: a comprehensive study," *SpringerPlus,* vol. 4, p. 645, 2015.

[7] O. Déniz, G. Bueno, J. Salido, and F. De la Torre, "Face recognition using Histograms of Oriented Gradients," *Pattern Recognition Letters,* vol. 32, pp. 1598-1603, 2011/09/01/ 2011.

[8] S. Moore and R. Bowden, "Local binary patterns for multi-view facial expression recognition," *Computer Vision and Image Understanding,* vol. 115, pp. 541-558, 2011/04/01/ 2011.

[9] D. Gabor, "Theory of communication. Part 1: The analysis of information," *Journal of the Institution of Electrical Engineers-Part III: Radio and Communication Engineering,* vol. 93, pp. 429-441, 1946.

[10] F. Zhang, Y. Song, W. Cai, M.-Z. Lee, Y. Zhou, H. Huang, *et al.*, "Lung nodule classification with multilevel patch-based context analysis," *IEEE Transactions on Biomedical Engineering,* vol. 61, pp. 1155-1166, 2014.

[11] H. Bay, T. Tuytelaars, and L. Van Gool, "Surf: Speeded up robust features," *Computer vision–ECCV 2006*, pp. 404-417, 2006.

[12] X. Tan and B. Triggs, "Fusing Gabor and LBP feature sets for kernel-based face recognition," in *International Workshop on Analysis and Modeling of Faces and Gestures*, 2007, pp. 235-249.

[13] C. Conde, D. Moctezuma, I. M. De Diego, and E. Cabello, "HoGG: Gabor and HoG-based human detection for surveillance in non-controlled environments," *Neurocomputing*, vol. 100, pp. 19-30, 2013.

[14] P. Ghosh and T. K. Taylor, "The Knee Joint Meniscus: A Fibrocartilage of Some Distinction," *Clinical orthopaedics and related research*, vol. 224, pp. 52-63, 1987.

[15] B. Seedhom, D. Dowson, and V. Wright, "Proceedings: Functions of the menisci. A preliminary study," *Annals of the rheumatic diseases*, vol. 33, p. 111, 1974.

[16] A. A. De Smet, M. Norris, D. Yandow, F. Quintana, B. Graf, and J. Keene, "MR diagnosis of meniscal tears of the knee: importance of high signal in the meniscus that extends to the surface," *AJR. American journal of roentgenology*, vol. 161, pp. 101-107, 1993.

[17] E. B. Dam, M. Lillholm, J. Marques, and M. Nielsen, "Automatic segmentation of high-and low-field knee MRIs using knee image quantification with data from the osteoarthritis initiative," *Journal of Medical imaging*, vol. 2, pp. 024001-024001, 2015.

[18] J. Fripp, P. Bourgeat, C. Engstrom, S. Ourselin, S. Crozier, and O. Salvado, "Automated segmentation of the menisci from MR images," in *Biomedical Imaging: From Nano to Macro, 2009. ISBI'09. IEEE International Symposium on*, 2009, pp. 510-513.

[19] M.-J. Kim, J.-H. Yoo, and H. Hong, "Automatic Segmentation of the meniscus based on Active Shape Model in MR Images through Interpolated Shape Information," *Journal of KIISE: Computing Practices and Letters*, vol. 16, pp. 1096-1100, 2010.

[20] A. Paproki, C. Engstrom, S. S. Chandra, A. Neubert, J. Fripp, and S. Crozier, "Automated segmentation and analysis of normal and osteoarthritic knee menisci from magnetic resonance images–data from the Osteoarthritis Initiative," *Osteoarthritis and Cartilage*, vol. 22, pp. 1259-1270, 2014.

[21] M. Swanson, J. Prescott, T. Best, K. Powell, R. Jackson, F. Haq, *et al.*, "Semi-automated segmentation to assess the lateral meniscus in normal and osteoarthritic knees," *Osteoarthritis and cartilage*, vol. 18, pp. 344-353, 2010.

[22] K. Zhang, W. Lu, and P. Marziliano, "The unified extreme learning machines and discriminative random fields for automatic knee cartilage and meniscus segmentation from multi-contrast MR images," *Machine vision and applications*, vol. 24, pp. 1459-1472, 2013.

[23] Y. Hata, S. Kobashi, Y. Tokimoto, M. Ishikawa, and H. Ishikawa, "Computer aided diagnosis system of meniscal tears with T1 and T2 weighted MR images based on fuzzy inference," *Lecture notes in computer science*, pp. 55-58, 2001.

[24] I. Boniatis, G. Panayiotakis, and E. Panagiotopoulos, "A computer-based system for the discrimination between normal and degenerated menisci from magnetic resonance images," in *Imaging Systems and Techniques, 2008. IST 2008. IEEE International Workshop on*, 2008, pp. 335-339.

[25] C. Köse, O. Gençalioğlu, and U. Şevik, "An automatic diagnosis method for the knee meniscus tears in MR images," *Expert Systems with Applications*, vol. 36, pp. 1208-1216, 3// 2009.

[26] B. Ramakrishna, W. Liu, G. Saiprasad, N. Safdar, C.-I. Chang, K. Siddiqui, *et al.*, "An automatic computer-aided detection system for meniscal tears on magnetic resonance images," *IEEE transactions on medical imaging*, vol. 28, pp. 1308-1316, 2009.

[27] J.-C. Fu, C.-C. Lin, C.-N. Wang, and Y.-K. Ou, "Computer-aided diagnosis for knee meniscus tears in magnetic resonance imaging," *Journal of Industrial and Production Engineering*, vol. 30, pp. 67-77, 2013.

[28] M. F. Zarandi, A. Khadangi, F. Karimi, and I. Turksen, "A Computer-Aided Type-II Fuzzy Image Processing for Diagnosis of Meniscus Tear," *Journal of digital imaging*, vol. 29, pp. 677-695, 2016.

[29] A. Saygili and S. Albayrak, "Meniscus segmentation and tear detection in the knee MR images by fuzzy c-means method," in *Signal Processing and Communications Applications Conference (SIU), 2017 25th*, 2017, pp. 1-4.

[30] D. Hayashi, F. W. Roemer, M. Jarraya, and A. Guermazi, "Imaging of Osteoarthritis," in *Geriatric Imaging*, ed: Springer, 2013, pp. 93-121.

[31] J. Belo, M. Berger, B. Koes, and S. Bierma-Zeinstra, "The prognostic value of the clinical ACR classification criteria of knee osteoarthritis for persisting knee complaints and increase of disability in general practice," *Osteoarthritis and cartilage*, vol. 17, pp. 1288-1292, 2009.

[32] A. Foundation. *What is Osteoarthritis ?* Available: http://www.arthritis.org/about-arthritis/types/osteoarthritis/what-is-osteoarthritis.php

[33] D. Schiphof, B. M. de Klerk, B. W. Koes, and S. Bierma-Zeinstra, "Good reliability, questionable validity of 25 different classification criteria of knee osteoarthritis: a systematic appraisal," *Journal of clinical epidemiology*, vol. 61, pp. 1205-1215. e2, 2008.

[34] H. Iijima, T. Aoyama, K. Nishitani, H. Ito, N. Fukutani, T. Isho, *et al.*, "Coexisting lateral tibiofemoral osteoarthritis is associated with worse knee pain in patients with mild medial osteoarthritis," *Osteoarthritis and cartilage*, vol. 25, pp. 1274-1281, 2017.

[35] A. Elbaz, A. Mor, G. Segal, R. Debi, N. Shazar, and A. Herman, "Novel classification of knee osteoarthritis severity based on spatiotemporal gait analysis," *Osteoarthritis and cartilage*, vol. 22, pp. 457-463, 2014.

[36] M. Edwards, J. Paccou, K. Ward, K. Jameson, C. Moss, J. Woolston, *et al.*, "The relationship of bone properties using high resolution peripheral quantitative computed tomography to radiographic components of hip osteoarthritis," *Osteoarthritis and cartilage*, vol. 25, pp. 1478-1483, 2017.

[37] S. Hardcastle, P. Dieppe, C. Gregson, N. Arden, T. Spector, D. Hart, *et al.*, "Individuals with high bone mass have an increased prevalence of radiographic knee osteoarthritis," *Bone*, vol. 71, pp. 171-179, 2015.

[38] M. Boesen, K. Ellegaard, M. Henriksen, H. Gudbergsen, P. Hansen, H. Bliddal, *et al.*, "Osteoarthritis year in review 2016: imaging," *Osteoarthritis and cartilage*, vol. 25, pp. 216-226, 2017.

[39] Y. Wang, A. Teichtahl, and F. M. Cicuttini, "Osteoarthritis year in review 2015: imaging," *Osteoarthritis and cartilage*, vol. 24, pp. 49-57, 2016.

[40] WebMD. *Knee Injury and Meniscus Tear*. Available: http://www.webmd.com/fitness-exercise/tc/meniscus-tear-topic-overview#1

[41] A. A. o. O. Surgeons. *Meniscus Tears*. Available: http://orthoinfo.aaos.org/topic.cfm?topic=a00358

[42] I. Rauscher, R. Stahl, J. Cheng, X. Li, M. B. Huber, A. Luke, *et al.*, "Meniscal Measurements of T1ρ and T2 at MR Imaging in Healthy Subjects and Patients with Osteoarthritis," *Radiology*, vol. 249, pp. 591-600, 2008.

[43] M. E. Bowers, G. A. Tung, B. C. Fleming, J. J. Crisco, and J. Rey, "QUANTIFICATION OF MENISCAL VOLUME BY SEGMENTATION OF 3T MAGNETIC RESONANCE IMAGES," *Journal of biomechanics*, vol. 40, pp. 2811-2815, 03/27 2007.

[44] S. S. Gornale, P. U. Patravali, K. S. Marathe, and P. S. Hiremath, "Determination of Osteoarthritis Using Histogram of Oriented Gradients and Multiclass SVM," *International Journal of Image, Graphics & Signal Processing*, vol. 9, 2017.

[45] A. Saygılı and S. Albayrak, "A new computer-based approach for fully automated segmentation of knee meniscus from magnetic resonance images," *Biocybernetics and Biomedical Engineering*, vol. 37, pp. 432-442, 2017.

[46] A. Saygili, H. Kaya, and S. Albayrak, "Automatic detection of meniscal area in the knee MR images," in *Signal Processing and Communication Application Conference (SIU), 2016 24th*, 2016, pp. 1337-1340.

[47] A. Tiulpin, J. Thevenot, E. Rahtu, and S. Saarakkala, "A novel method for automatic localization of joint area on knee plain radiographs," in *Scandinavian Conference on Image Analysis*, 2017, pp. 290-301.

[48] D. Huang, C. Shan, M. Ardabilian, Y. Wang, and L. Chen, "Local binary patterns and its application to facial image analysis: a survey," *IEEE Transactions on Systems, Man, and Cybernetics, Part C (Applications and Reviews)*, vol. 41, pp. 765-781, 2011.

[49] M. A. Finnilä, J. Thevenot, O. M. Aho, V. Tiitu, J. Rautiainen, S. Kauppinen, *et al.*, "Association between subchondral bone structure and osteoarthritis histopathological grade," *Journal of Orthopaedic Research*, vol. 35, pp. 785-792, 2017.

[50] J. Thevenot, J. Chen, M. Finnilä, M. Nieminen, P. Lehenkari, S. Saarakkala, *et al.*, "Local binary patterns to evaluate trabecular bone structure from micro-CT data: application to studies of human osteoarthritis," in *European Conference on Computer Vision*, 2014, pp. 63-79.

[51] M. Pietikäinen, A. Hadid, G. Zhao, and T. Ahonen, "Local binary patterns for still images," in *Computer vision using local binary patterns*, ed: Springer, 2011, pp. 13-47.

[52] T. Ojala, M. Pietikainen, and T. Maenpaa, "Multiresolution gray-scale and rotation invariant texture classification with local binary patterns," *IEEE Transactions on pattern analysis and machine intelligence*, vol. 24, pp. 971-987, 2002.

[53] Z.-G. Liu, Y. Yang, and X.-H. Ji, "Flame detection algorithm based on a saliency detection technique and the uniform local binary pattern in the YCbCr color space," *Signal, Image and Video Processing*, vol. 10, pp. 277-284, February 01 2016.

[54] M. Nevitt, D. Felson, and G. Lester, "The osteoarthritis initiative," in *Protocol for the Cohort Study*, ed, 2009 http://oai.epi-ucsf.org/datarelease/docs/StudyDesignProtocol.pdf.

[55] K. Bloecker, A. Guermazi, W. Wirth, C. K. Kwoh, H. Resch, D. J. Hunter, *et al.*, "Correlation of semiquantitative vs quantitative MRI meniscus measures in osteoarthritic knees: results from the Osteoarthritis Initiative," *Skeletal Radiology*, vol. 43, pp. 227-232, February 01 2014.